Internal electronic structure and fine structure of multiexcitons in semiconductor quantum dots

Vladan Mlinar and Alex Zunger*
National Renewable Energy Laboratory, Golden, Colorado 80401, USA
(Received 17 July 2009; revised manuscript received 6 October 2009; published 12 November 2009)

We perform a detailed theoretical study of the characteristic internal electronic structure of various multiexcitons (N_h,N_e), where N_h is number of holes and N_e is the number of electrons in the self-assembled semiconductor quantum dots (QDs). For each of the leading (N_h,N_e) excitonic complexes we start from the single-particle configuration (e.g., a specific occupation pattern of S and P electron and hole levels by a few carriers) and then show the many-particle multiplet levels for the initial state of emission (N_h,N_e) and the final state of emission $(N_h-1,\ N_e-1)$. We denote which states are dark and which are bright; the order and multiplicity, the leading single-particle character of each multiplet state, and the fine-structure splittings. These are of general utility. We also show explicit numerical values for distances between various transitions for four specific QDs. Here the presented information is important and potentially useful for a few reasons: (i) the information serves as a guide for spectroscopic interpretation; (ii) the information reveals non-Aufbau cases, where the dot does not have Aufbau occupation of carriers' levels; (iii) the information shows which transitions are sensitive to random-alloy fluctuations (if the dot is alloyed) and importance of this effect. We show that because of such alloy information, distances between peaks cannot be used to gauge structural information.

DOI: 10.1103/PhysRevB.80.205311 PACS number(s): 73.21.La, 78.67.Hc, 68.65.−k

I. INTRODUCTION

Advances in the synthesis and spectroscopy of self-assembled semiconductor quantum dots (QDs) now routinely reveal a rich set of very sharp excitonic lines in a single-dot emission spectrum.[1–12] These lines originate from optical transitions between various many-carrier configurations, $(N_h,N_e)\rightarrow(N_h-1,N_e-1)$, where single electron-hole (e-h) pair recombines radiatively in the presence of the other N_h-1 and N_e-1 "spectator" carriers. Whereas in single-particle physics (e.g., band structure of solids) such transitions would be expressed as the difference between electron levels and hole levels (single-particle band gaps), in nanostructures there are additional dominant terms of carrier-carrier repulsion, exchange, and correlations, leading to many more lines than anticipated from the single-particle picture. The emission spectrum of each exciton complex (N_h,N_e) has a characteristic number of spectral lines, positions in the spectra, and intensities. Such a multiexcitonic spectrum encodes in it information about the Coulomb interactions between carriers, including exchange and correlation effects,[8,10] thus revealing many-particle physics in confined spaces. Exchange interactions between carriers in the QD lift the degeneracy of multiexciton energy levels. For example, electron-hole exchange interaction splits the exciton ground state into four levels, one doubly degenerate that is optically inactive ("dark"), and two optically active ("bright") levels (see, e.g., Ref. 13). The splitting between the two optically active states is called the fine-structure splitting (FSS). A similar situation occurs in the case a dot is charged with more than one electron and hole, except that the number of lines may differ from the simple case of neutral monoexciton.

Experimentally, various multiexcitons have been identified unambiguously in the emission spectra of individual QDs either by tuning the excitation intensity[2] or direction and amplitude of an electric field, in which the dot is embedded.[1,9,11,12] However, the interpretation of such results in terms of the internal electronic structure and fine structure (FS) is limited by the lack of reliable theoretical assignment of the emission lines in the spectra. Also, dark states are not accessible in the absence of an external magnetic field and require theory to predict dark bright states' splittings. Theoretical models based on perturbation theory[2,14] disregard QD morphology and determine the spectroscopic features by considering only a single configuration (an assignment of electron and hole occupations to electron and hole levels) for the initial and the final states. These appealing intuitive approaches relate simply the initial and final single-particle configurations with the many-particle transition energies, but are often not able to interpret the internal structure and fine structure. More complex theoretical models allow configuration mixing in the initial and final many-particle states and take into account QD structure (geometry and composition profile), strain, and piezo effects.[7–9,12,15–17] Here we use a state-of-the-art atomistic many-body pseudopotential method[18,19] and demonstrate how and where the simple perturbation-theory-based models fail, and provide simple schematic plots showing for each neutral or charged multiexciton the relevant single particle as well as multiparticle multiplets needed to interpret such states. *Thus, we will provide a detailed account of the genesis of observable many-electron multiples from (dominant) single-particle levels.* Also, we will illustrate that the internal structure and FS of multiexcitons are sensitive to QD structural properties. Simple arguments cannot be used to understand the structure-spectra relationship and artificial intelligence methods are required. For example, a procedure for finding structure-spectra relationship in QDs was proposed recently in Ref. 20, where we focused on a smaller subset of spectral lines, calculated them for ~240 different dot structures, and addressed the issue of finding data-mining-like correlations between structure and sequence of spectral lines.

The purpose of this work is to provide an insight into the characteristic internal electronic structure of various multiexcitons in generic QDs, and to serve as a guide for experimen-

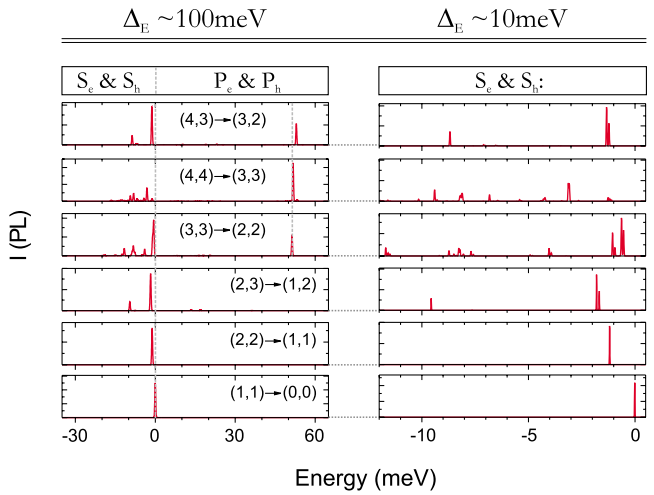

FIG. 1. (Color online) Calculated emission spectra of a lens-shaped $In_{0.6}Ga_{0.4}As/GaAs$ QD with $2R=25.2$ nm and $h=3.5$ nm for different exciton occupations shown on two different energy scales: on a $\Delta_1 \approx 100$ meV scale and on a $\Delta_1 \approx 10$ meV scale. Energies are given relative to the monoexciton energy, $E_X^0 = 1.255$ eV. Gray dashed lines show the position of the $(1,1) \rightarrow (0,0)$ monoexciton peak and the position of the $P_e \& P_h(3,3) \rightarrow (2,2)$ peak.

tal interpretation. Indeed, the origin of the various lines is difficult to guess without a many-body calculation. Thus, for each of the leading (N_h, N_e) excitonic complexes we will start from the single-particle configuration (e.g., a specific occupation pattern of S and P electron and hole levels by a few carriers) and then show the final result of the many-body treatment, i.e., the many-particle (multiplet) levels for (N_h, N_e) (=the initial state of emission) and $(N_h-1,\ N_e-1)$ (=the final state of emission). We will denote which states are dark and which are bright; the order, multiplicity and the leading single-particle character of each multiplet state, and the FSS. The schematic transitions for multiexcitons pertain to a generic self-assembled QD and are of general validity according to our calculations. The specific energy separations between transition lines are determined by structural parameters of QDs (shown in Tables within figures for each multiexciton) and also by random-alloy fluctuations. We provide numerical results for four prototypical structures and note that all other inspected structures follow this range.

Here the presented information is important and potentially useful for a few reasons: (i) the information serves as a guide for spectroscopic interpretation; (ii) the information reveals non-Aufbau cases, where the dot does not have Aufbau occupation of carriers' levels; (iii) the information shows which transitions are sensitive to random-alloy fluctuations (if the dot is alloyed) and importance of this effect. We show that because of such alloy information, distances between peaks cannot be used to gauge structural information.

II. BASIC FEATURES OF THE MULTIEXCITONIC SPECTRA

A. Exciton complexes in quantum dots

Loading a QD with N_h holes and N_e electrons creates either neutral (multi)excitons (if $N_h=N_e$) or charged (multi-)excitons (if $N_h \neq N_e$). For example, a neutral monoexciton X^0 has one hole and one electron $[(N_h=1;\ N_e=1)]$; a nega-

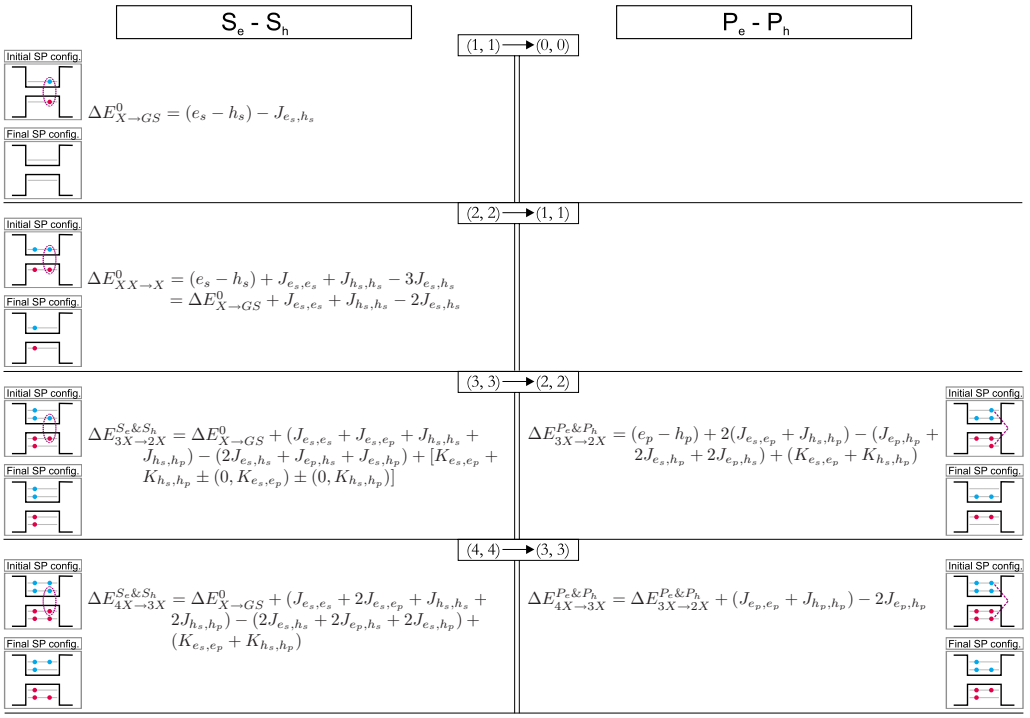

FIG. 2. (Color online) Excitonic recombination energies in the perturbation-theory approximation in terms of e-e, h-h, and e-h Coulomb energies ($J_{es,es}$, $J_{es,ep}$, $J_{hs,hs}$, $J_{es,hs}$, etc.,) and e-e and h-h exchange energies ($K_{es,ep}$, $K_{hs,hp}$, etc.,) under the assumption that spin-orbit coupling is negligible.

tive trion X^{-1} has one hole and two electrons [labeled (1,2)]; and a positively charged biexciton XX^{+1} has three holes and two electrons (3,2), etc.

S channel radiative recombination ($S_e \& S_h$) occurs when an electron in the S_e level recombines with a hole in the S_h level. When a P electron recombines with a P hole, there is a P recombination channel, denoted as $P_e \& P_h$. The $S_e \& S_h$ and $P_e \& P_h$ recombination channels are shifted due to the ϵ_s-ϵ_p single-particle gap.

In the self-assembled QDs the recombination of a single electron-hole pair in the presence of other N_e-1 and N_h-1 carriers leads to a radiative emission from all other states, and thus to a rich observable multiexcitonic spectra. In other (colloidal) QDs, often the recombination of an electron with a hole leads to a faster (~ps) nonradiative Auger excitation of some of the spectator particles, thus multiexciton emission is not always seen.[21,22]

B. Low-resolution versus high-resolution multiexcitonic spectra

Figure 1 shows typical calculated spectra of an (In,Ga)As QD (method is discussed in Sec. III A). Each multiexciton line is split into a set of multiplets separated by FSS. On ~100 meV energy span (left panel in Fig. 1) we see a low-resolution energy scale, where the emission spectra from a (N_h,N_e) multiexciton system can be seen only as a single emission line (singlet) or multiple emission lines (multiplets).[2,17] On the other hand, higher resolution ~10 meV energy scale spectra, depicted in Fig. 1 (right panel), resolves most of the multiplets of the multiexcitonic transitions. For example, $(2,3)\rightarrow(1,2)$ transition has only two peaks resolved on low-energy scale (left panel in Fig. 1), whereas higher resolution spectra (right panel in Fig. 1) reveal three emission lines. Indeed, it now becomes possible to resolve FSS on the μeV resolution, e.g., Seidl *et al.* in Ref. 23 measured FSS of monoexciton with the accuracy as high as 4 μeV.

C. Simplified perturbation-theory-based rules for the interpretation of the low-resolution spectra

The basic low-resolution features of multiexcitonic spectra have been traditionally interpreted using perturbation theory.[24] In this approach one disregards QD morphology and determines the spectroscopic features by considering only a single configuration (an assignment of electron and hole occupations to electron and hole levels) for the initial and the final states, i.e., by neglecting correlation effects. This intuitive approach relates simply the initial and final single-particle configurations with the many-particle transition energies. Figure 2 illustrates the expressions for the excitonic recombination energies within the perturbation-theory approximation in terms of the repulsive Coulomb electron-electron (e-e) ($J_{es,es}$, $J_{es,ep}$, $J_{ep,ep}$, etc.,) and hole-hole (h-h) ($J_{hs,hs}$, $J_{hs,hp}$, $J_{hp,hp}$, etc.,) energies, as well as the attractive Coulomb electron-hole ($J_{es,hs}$, $J_{es,hp}$, $J_{ep,hs}$, etc.,) energies, where s and p denote the orbital character, e is the electron, and h is the hole. Contributions from electron-electron and hole-hole exchange energies ($K_{es,ep}$, $K_{es,ep2}$, $K_{hs,hp}$, $K_{hs,hp2}$, etc.,) are also given in Fig. 2. In this simple approach one neglects spin-orbit coupling as well as electron-hole exchange energies since $K_{e,h} \ll K_{e,e}$; $K_{h,h}$.[2,14] This approach counts the number of electron-electron, hole-hole, and electron-hole interactions and formulate the transition energies on this basis, assuming universal interaction energies. For example, the $(2,2)\rightarrow(1,1)$ transition, where the initial single-particle configuration is $h_0^2 e_0^2$ and the final single-particle configuration is $h_0^1 e_0^1$, gives a transition energy $\Delta E[(2,2)\rightarrow(1,1)]$ that equals the "band gap" $\epsilon(e_0)$-$\epsilon(h_0)$ plus $(J_{e,e}+J_{h,h}-3J_{e,h})$. As we shall see later in Fig. 4, the situation is much more complicated as one goes beyond this simple picture.

The perturbation-theory approximation leads to two general predictions:[17] first, it predicts when a $(N_h,N_e)\rightarrow(N_h-1,N_e-1)$ multiexcitonic spectrum will consist of a single dominant line (singlet) or exhibit a manifold of lines (multiplet). If in the final state there is a maximum of one partially occupied hole and one partially occupied electron level, the $(N_h,N_e)\rightarrow(N_h-1,N_e-1)$ spectrum will consist of a single line; otherwise multiple lines are expected. Figure 2 illustrates this prediction for the $(N_h,N_e)\rightarrow(N_h-1,N_e-1)$ transitions. Singlet spectra for the S-channel case are: $(1,1)\rightarrow(0,0)$, $(2,2)\rightarrow(1,1)$, and $(4,4)\rightarrow(3,3)$; and for the P-channel case are: $(3,3)\rightarrow(2,2)$ and $(4,4)\rightarrow(3,3)$. Multiplets are expected for the S-channel case: $(3,3)\rightarrow(2,2)$.

Second, the expressions shown in Fig. 2 suggest that under well-defined approximations all singlet transition ener-

TABLE I. Four model QDs represented as a set of four structural motifs: QD base length (b), height (h), and indium composition ($\bar{X}_{In}$). All dots are sitting on two monolayer wetting layer. Last three columns show exciton energy (E_X^0), and P shell splitting of electrons (δe_p) and holes (δh_p), respectively. For elongated lens model QD, the base is elliptic with $b1/b2=1.25$ and $(b1+b2)/2=30$ nm, where $b1$ and $b2$ are axes of the ellipse.

Dot/Structural motif	Shape	b (nm)	h (nm)	$\bar{X}_{In}$ (%)	E_X^0 (eV)	δe_p (meV)	δh_p (meV)
Dot A	Lens	25	3.5	60	1.255	2.351	4.383
Dot B	Truncated cone	25	3.0	80	1.101	0.627	0.702
Dot C	Lens	23	2.0	100	1.094	1.720	8.456
Dot D	Elongated lens in $[1\bar{1}0]$	30	5.0	60	1.198	8.903	2.404

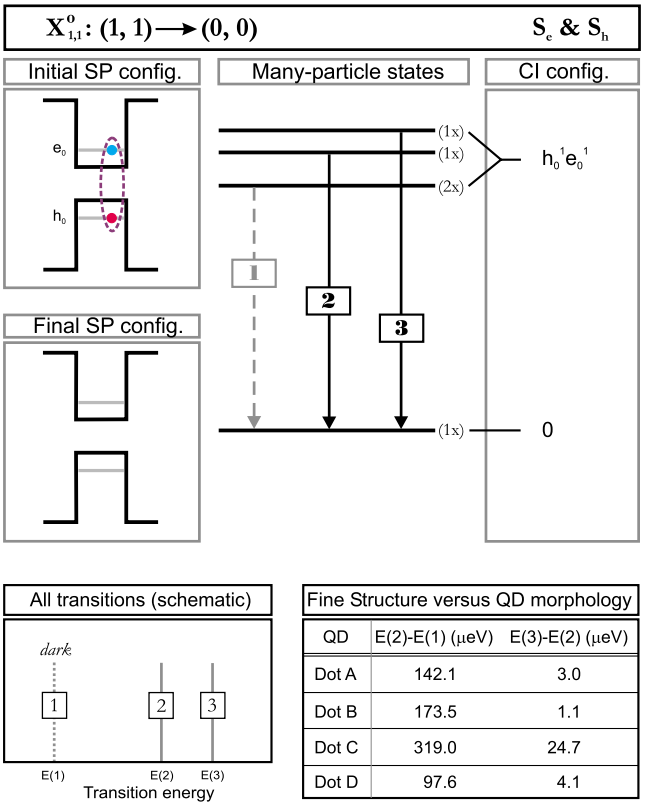

Fine Structure versus QD morphology

QD	E(2)-E(1) (μeV)	E(3)-E(2) (μeV)
Dot A	142.1	3.0
Dot B	173.5	1.1
Dot C	319.0	24.7
Dot D	97.6	4.1

FIG. 3. (Color online) Schematic plot of the internal electronic structure of monoexciton (N_h=1, N_e=1). The title indicates the transition [e.g., (1,1)→(0,0)] and the recombination channel. The left panels give the initial single-particle levels and the final single-particle level; the dotted ellipse indicates the e-h pair that recombines. The center panels give the initial many-particle multiplets and final many-particle multiplets and their multiplicities. On the RHS we give the dominant CI configuration denoted as $h_0^{n0}h_1^{n1}\ldots h_j^{nj}e_0^{m0}e_1^{m1}\ldots e_i^{mi}$, where i and j denote electron and hole levels, respectively, and $mj(ni)$ denote number of electrons (holes) on level $i(j)$ ($0\leq ni$, $mj\leq 2$). The vertical arrows connecting final and initial multiplets show the multiexcitonic transition. The dashed lines denote dark transitions. Bottom left gives schematically the spectra of all (allowed+forbidden) transitions. The Table gives an idea about the range of FSS for different QD structures, where the energies are given in μeV.

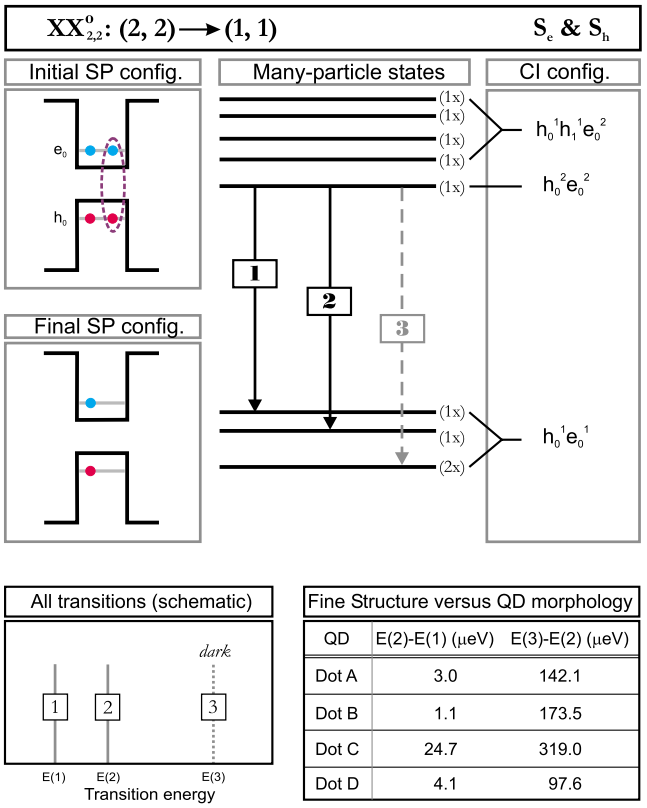

Fine Structure versus QD morphology

QD	E(2)-E(1) (μeV)	E(3)-E(2) (μeV)
Dot A	3.0	142.1
Dot B	1.1	173.5
Dot C	24.7	319.0
Dot D	4.1	97.6

FIG. 4. (Color online) Schematic plot of the internal electronic structure of biexciton (N_h=2, N_e=2).

gies for different $(N_h,N_e)\rightarrow(N_h-1,N_e-1)$ spectra within the same recombination channel will align energetically.[17] Examples in Fig. 2 include for the S_e-S_h recombination channel $(1,1)\rightarrow(0,0)$, $(2,2)\rightarrow(1,1)$, and for the P_e-P_h recombination channel $(3,3)\rightarrow(2,2)$ and $(4,4)\rightarrow(3,3)$.

This simple perturbative approach has been especially attractive because of its simplicity and remarkable predictive power. However, this approach fails to predict singlet vs multiplet for $(3,3)\rightarrow(2,2)$ and $(4,4)\rightarrow(3,3)$ transitions, regardless of QD morphology, and is insensitive to the FSS on $\sim\mu$eV energy scale.[17] For example, according to the perturbation theory, P-channel $(3,3)\rightarrow(2,2)$ transition is a singlet, but in the full calculations there are actually two optically active transitions split by several tens μeV [see Sec. IV C]. Therefore, interpretation of the spectra using the perturbation theory is partially successful on "low-resolution" ~100 meV spectra, but is insensitive to FSS on sub-meV scale.

III. THEORETICAL APPROACH

In this paper we discuss the internal electronic structure and FSS of neutral, positively charged, and negatively charged (multi)excitons going beyond the simple perturbative approach explained in Sec. II C. We employ here an atomistic many-body pseudopotential method in order to provide a detailed account of the genesis of observable many-electron multiplets from (dominant) single-particle levels.

A. Method

For the assumed size, shape, and composition of a QD we first relax the atomic position $\{\mathbf{R}_{i,\alpha}\}$ via the valence force field method[25] within the simulation supercell of $\sim 2\times 10^6$ atoms (QD+GaAs matrix). Screened-strain-dependent atomic pseudopotential $v_\alpha[\mathbf{r};Tr(\epsilon)]$ is placed on each site of atom of type α. They are fitted to bulk properties of InAs and GaAs, including bulk band structures, experimental deformation potentials and effective masses and directly feel strain effects via hydrostatic component of the strain tensor $[Tr(\epsilon)]$. The total pseudopotential of the system $V(\mathbf{r})$ is constructed by superposing the nonlocal spin-orbit interaction, V_{so}, to the local-screened pseudopotential, $v_\alpha[\mathbf{r};Tr(\epsilon)]$, of all atoms[18]

$$V(\mathbf{r}) = V_{so} + \sum_{i,\alpha} v_\alpha[\mathbf{r} - \mathbf{R}_{i,\alpha}; Tr(\epsilon)]. \quad (1)$$

The single-particle electron $\{e_0, e_1, e_2, \ldots\}$ and hole $\{h_0, h_1, h_2, \ldots\}$ states are extracted from the single-particle Schrödinger equation[18]

$$[-1/2\nabla^2 + V(\mathbf{r})]\psi_i = E_i\psi_i. \quad (2)$$

The single-particle Hamiltonian includes quantum confinement effects, multiband coupling (conduction band, heavy hole, and light hole), intervalley coupling ($\Gamma - X - L$), strain effects, and spin-orbit coupling. Multiexciton complexes are calculated using the configuration-interaction (CI) method.[24] Slater determinants $\Phi_{v,c}$ are constructed from s, p, and d electron and hole orbitals (well separated in energy from the remaining dot-confined states), which give 12 electron and 12 hole single-particle states (counting spin). The multiexciton wave functions Ψ are expanded in terms of this determinal basis set. Our CI calculations are convergent both in the energetic positions of peaks in the spectra and intensity of the peaks (for detail see Ref. 17). The matrix elements of the many-particle Hamiltonian H in the basis set $\{\Psi_{v,c}\}$ are calculated as

$$H_{v,c,v',c'} = \langle \Phi_{v,c}|H|\Phi_{v',c'}\rangle = (E_c - E_v)\delta_{v,v'}\delta_{c,c'} - J_{vc,v'c'} + K_{vc,v'c'}, \quad (3)$$

where J and K are the Coulomb and exchange integrals, respectively

$$J_{vc,v'c'} = e^2 \sum_{\sigma_1,\sigma_2} \int\int \frac{\psi^*_{v'}(\mathbf{r}_1,\sigma_1)\psi^*_c(\mathbf{r}_2,\sigma_2)\psi_v(\mathbf{r}_1,\sigma_1)\psi_{c'}(\mathbf{r}_2,\sigma_2)}{\bar{\epsilon}(\mathbf{r}_1,\mathbf{r}_2)|\mathbf{r}_1,\mathbf{r}_2|} \times d\mathbf{r}_1 d\mathbf{r}_2, \quad (4)$$

$$K_{vc,v'c'} = e^2 \sum_{\sigma_1,\sigma_2} \int\int \frac{\psi^*_{v'}(\mathbf{r}_1,\sigma_1)\psi^*_c(\mathbf{r}_2,\sigma_2)\psi_{c'}(\mathbf{r}_1,\sigma_1)\psi_v(\mathbf{r}_2,\sigma_2)}{\bar{\epsilon}(\mathbf{r}_1,\mathbf{r}_2)|\mathbf{r}_1,\mathbf{r}_2|} \times d\mathbf{r}_1 d\mathbf{r}_2. \quad (5)$$

Coulomb and exchange integrals [Eqs. (4) and (5)] are computed numerically from the pseudopotential single-particle orbitals. The screening function for these integrals $\bar{\epsilon}(\mathbf{r}_1,\mathbf{r}_2)$ contains an ionic and an electronic component that exhibit a smooth transition from unscreened at short range to screened at long range.[19]

After we obtain the multiexciton states from the CI calculations, we analyze the CI configuration that has a major contribution to the CI state. This is called the dominant CI contribution. The emission spectra is calculated using Fermi's golden rule applied to the CI states, where configuration mixing in the initial and final states are reflected through the variation in energetic positions and intensities of the emission lines.

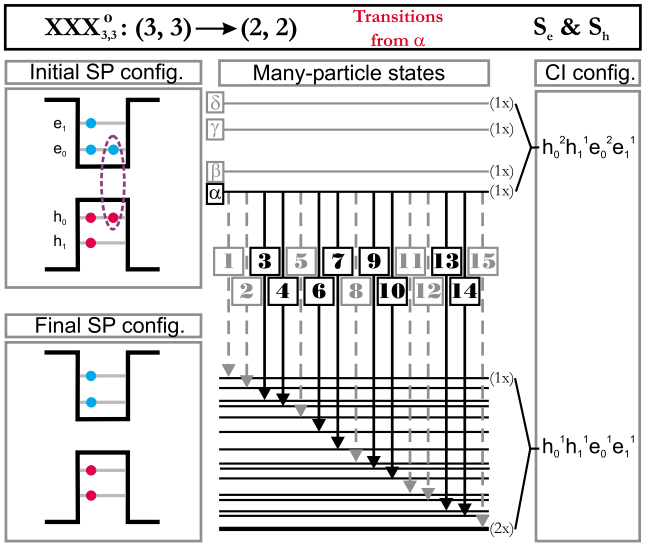

FIG. 5. (Color online) Schematic plot of the internal electronic structure of neutral triexciton (N_h=3, N_e=3). The S recombination channel of (3,3)→(2,2) transition from α multiexciton state is shown. The thick line in the final state corresponds to a doubly degenerate state, whereas the thin lines show single degenerate states.

B. Model quantum dots

Our model QDs are defined through four structural motifs: base length (b), height (h), shape, and average indium composition ($\bar{X}_{In}$). We use four model QDs, denoted as Dot A, Dot B, Dot C, and Dot D, as shown in Table I. For each of our four model QDs, we show exciton energy (E_X^0) and P-shell splitting of electrons and holes (last three columns in Table I). These model QDs are used to illustrate how morphology influences the internal electronic structure and FS of multiexcitons considered in the following sections.

IV. NEUTRAL (MULTI)EXCITONS

Figures 3–11 show schematic plots of the internal electronic structure of (N_h, N_e) multiexciton for N_h=N_e. The structure of each figure is as follows. The title indicates the transition [e.g., (2,2)→(1,1)] and the recombination channel. The left panels give the initial single-particle levels, e.g., $h_0^2e_0^2$ and the final single-particle level, e.g., $h_0^1e_0^1$; the dotted ellipse indicates the electron-hole pair that recombines. The center panels give the initial many-particle multiplets and final many-particle multiplets and their multiplicities. On the right-hand side (RHS) we give the dominant CI configuration. The vertical arrows connecting final and initial multiplets show the multiexcitonic transition. The dashed lines denote dark transitions. Bottom left position gives schematically the spectra of all (allowed+forbidden) transitions.

The schematic transitions illustrated in Figs. 3–11 pertain to a generic self-assembled QD and are of general validity according to our calculations. The specific energy separations between transition lines are determined by structural parameters of QDs (shown in Tables within the figures for each neutral multiexciton, where the energies are given in

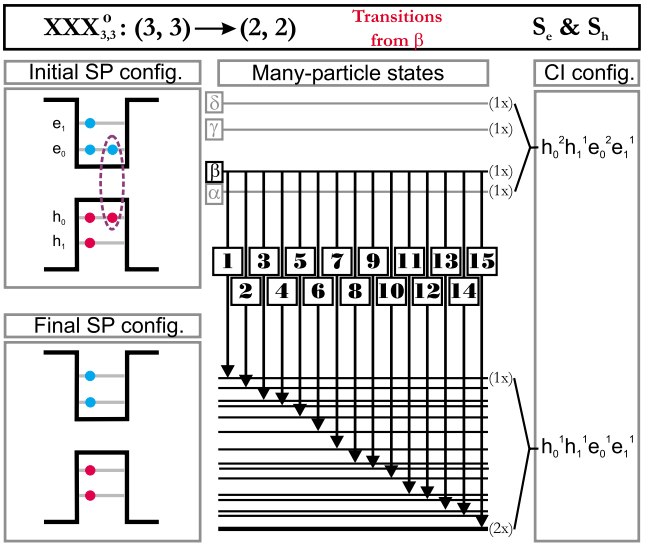

FIG. 6. (Color online) Schematic plot of the internal electronic structure of neutral triexciton (N_h=3, N_e=3). The S recombination channel of (3,3)→(2,2) transition from β multiexciton state is shown.

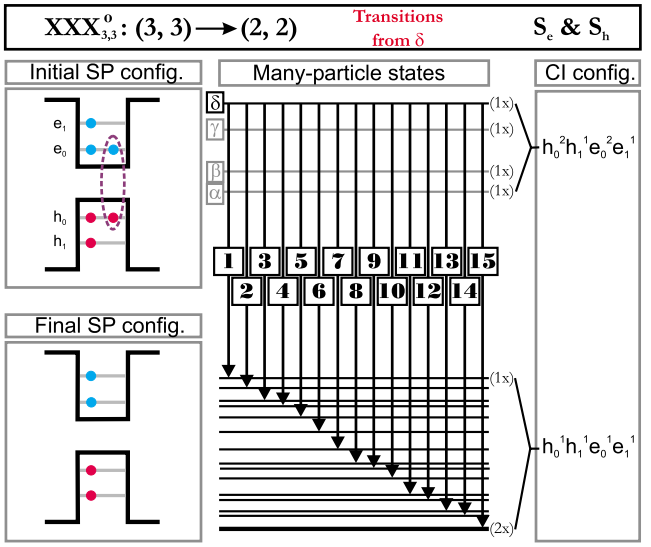

FIG. 8. (Color online) Schematic plot of the internal electronic structure of neutral triexciton (N_h=3, N_e=3). The S recombination channel of (3,3)→(2,2) transition from δ multiexciton state is shown.

μeV] and also by random-alloy fluctuations (see Sec. VII). We provide numerical results for our four prototypical structures and note that all other inspected structures follow this range.

A. $X^0_{1,1}$: Neutral exciton (Fig. 3)

The simplest case of e-h recombination is the monoexciton (N_h=1, N_e=1) shown in Fig. 3. The initial single-particle level has one electron (blue/gray) in the conduction band and one hole in the valence band (red/dark gray). Including spin, each of these states has a multiplicity of two, so the electron-hole exciton has a multiplicity of 2×2=4. The central part shows many-particle initial states. The electron-hole exchange interaction causes splitting into 2+1+1 multiplets, where the lowest state (2×) is dark (see e.g., Ref. 13) and there are two optically active states. The final many-

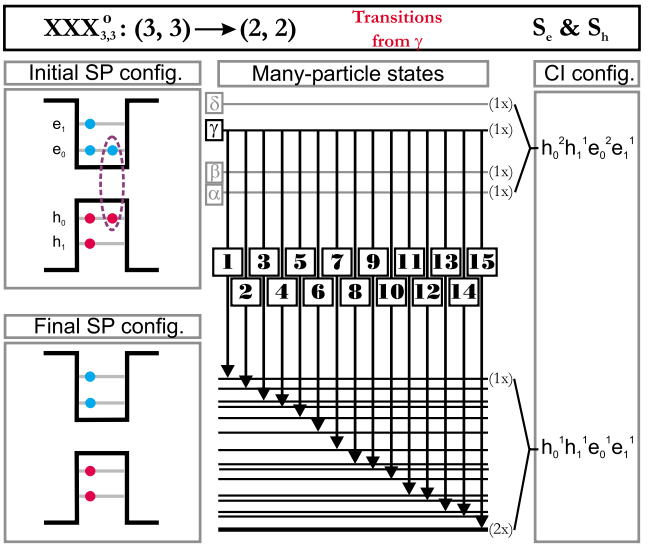

FIG. 7. (Color online) Schematic plot of the internal electronic structure of neutral triexciton (N_h=3, N_e=3). The S recombination channel of (3,3)→(2,2) transition from γ multiexciton state is shown.

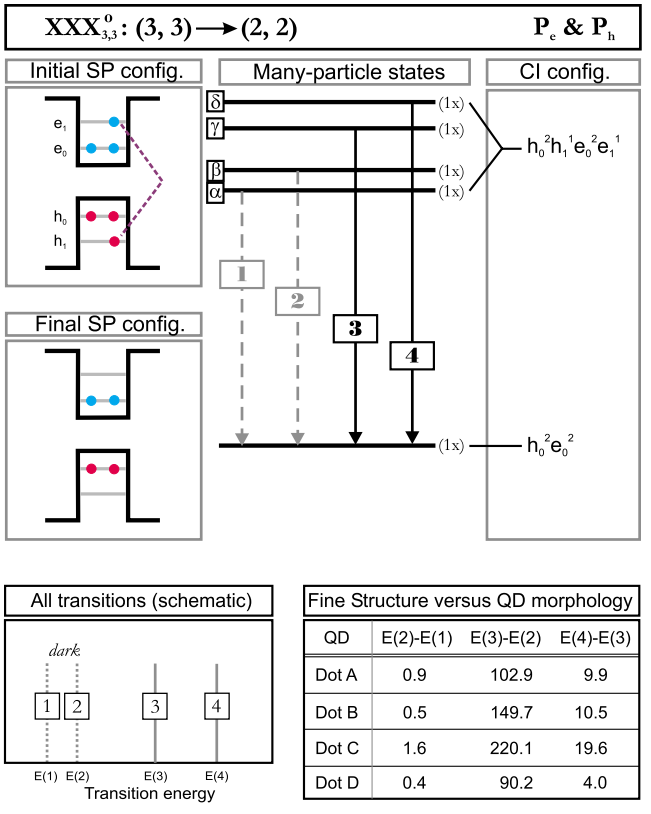

Fine Structure versus QD morphology			
QD	E(2)-E(1)	E(3)-E(2)	E(4)-E(3)
Dot A	0.9	102.9	9.9
Dot B	0.5	149.7	10.5
Dot C	1.6	220.1	19.6
Dot D	0.4	90.2	4.0

FIG. 9. (Color online) Schematic plot of the internal electronic structure of neutral triexciton (N_h=3, N_e=3). The P recombination channel of (3,3)→(2,2) transition is shown.

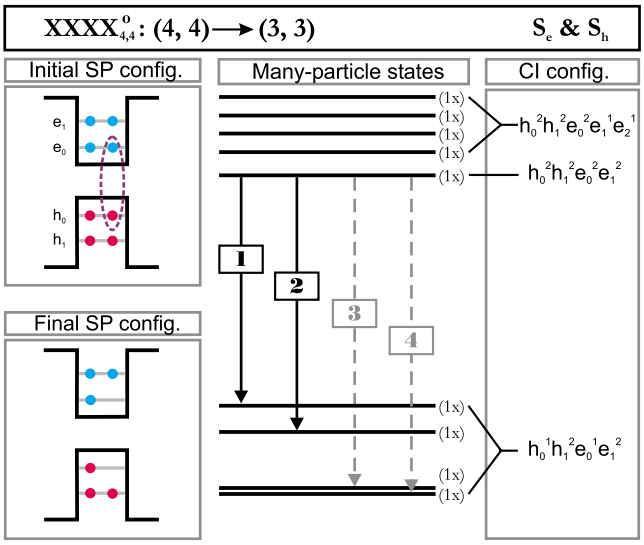

Fine Structure versus QD morphology			
QD	E(2)-E(1)	E(3)-E(2)	E(4)-E(3)
Dot A	50.1	30.3	9.8
Dot B	8.0	42.2	0.4
Dot C	19.7	40.2	1.2
Dot D	10.1	48.2	9.0

FIG. 10. (Color online) Schematic plot of the internal electronic structure of neutral four-exciton (N_h=4, N_e=4). The S recombination channel of (4,4)→(3,3) transition is shown.

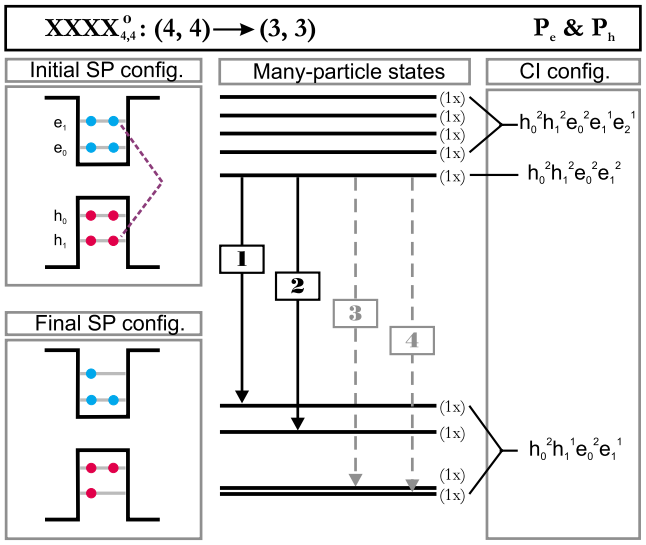

Fine Structure versus QD morphology			
QD	E(2)-E(1)	E(3)-E(2)	E(4)-E(3)
Dot A	10.0	107.3	0.1
Dot B	8.0	160.1	0.5
Dot C	20.1	219.8	1.6
Dot D	10.3	80.2	0.3

FIG. 11. (Color online) Schematic plot of the internal electronic structure of neutral four-exciton (N_h=4, N_e=4). The P recombination channel of (4,4)→(3,3) transition is shown.

particle state corresponds to a single multiplet due to h^0e^0. Thus, the intermultiplet transition 1, denoted by gray dashed line, is not optically active; there are two optically active transitions marked 2 and 3 (solid lines). Transitions 2 and 3 are linearly polarized along orthogonal axis.[26] The splitting between these two bright states, i.e., the FSS, is usually on the order of a few tens of μeV and is determined by QD structural properties.[13] We show the values of the FSS for four model dots in the Table within Fig. 1.

B. $XX^0_{2,2}$: Neutral biexciton (Fig. 4)

The initial single-particle level is $h_0^2e_0^2$ and the final one is $h_0^1e_0^1$ (Fig. 4). The initial multiplet state of $XX^0_{2,2}$ consists of one single degenerate state given that it is not split by the exchange interaction. This is so because the net spin of the involved electrons and holes is zero. The final multiplet state has two single degenerate and one doubly degenerate, all dominated by $h_0^1e_0^1$. The (2,2)→(1,1) decay involves two allowed transitions with the final states being the bright states of the X^0, as shown in Fig. 4. Therefore, the FSS of neutral exciton is reproduced, yet inverted in the XX^0 to X^0 decay (compare center panels of Figs. 3 and 4).

Figure 4 shows the spectrum of the biexciton in the ground state, i.e., when both electrons and both holes are in the ground state. However, it is possible that one of the holes is in the excited state. This can happen if the initial multiplet state, with dominant configuration $h_0^2e_0^2$ is very close in energy to the first excited initial state with dominant configuration $h_0^1h_1^1e_0^2$. In that case the net spin is 2^2=4, which leads to two emission lines in the spectra.[27,28]

C. $XXX^0_{3,3}$: Neutral triexciton (Figs. 5–9)

When a dot is loaded with more than two electrons and two holes (N_h>2, N_e>2), there is also a P recombination channel (P_e&P_h), where the P electron can recombine with the P hole (see Sec. II A). In what follows, we discuss both recombination channels.

1. S_e-S_h recombination channel

In the case of triexciton ($XXX^0_{3,3}$), the single-particle S-electron and S-hole levels are fully occupied, and the P level is only partially occupied (Fig. 5). This leads to the total multiplicity of four for $XXX^0_{3,3}$. Thus, the initial state of (3,3) multiexciton level splits into four levels, denoted as α, β, γ, and δ, all dominated by the $h_0^2h_1^1e_0^2e_0^1$ configuration. When a S electron and a S hole of the (3,3) multiexciton recombine, the final multiexcitonic state has a dominant configuration $h_0^1h_1^1e_0^1e_0^1$, i.e., with one electron in S and one in P level (same with the holes). This means that the spin of the particles are independent, allowing 2^4=16 different spin configurations. The total multiplicity of the final multiparticle state is 16. Thus, the S recombination channel of (3,3) →(2,2) transitions has 64 transitions. Because of this large number of transitions, we analyze the transitions from each

TABLE II. Energy separations between the transitions of (3,3) multiexciton as they vary with QD morphology for emission from α and β states (see Figs. 5 and 6). Energies are given in μeV.

	Transitions from α				Transitions from β			
Trans	Dot A	Dot B	Dot C	Dot D	Dot A	Dot B	Dot C	Dot D
E(2)-E(1)	2775.5	4.6	2991.1	2009.1	2776.4	5.1	2992.8	2009.5
E(3)-E(2)	569.9	12.8	1031.1	2021.0	570.8	13.3	1032.8	2021.4
E(4)-E(3)	57.2	1553.8	8.8	1.9	58.1	1554.3	10.5	2.3
E(5)-E(4)	4170.9	10.9	6329.6	8324.1	4171.8	11.4	6331.3	8324.5
E(6)-E(5)	3.6	3540.9	9.9	9.1	4.5	3541.4	11.6	9.5
E(7)-E(6)	0.3	234.4	2.8	9.6	1.2	234.9	4.5	10.0
E(8)-E(7)	2972.5	13.3	3521.2	7338.1	2973.4	13.8	3522.9	7338.5
E(9)-E(8)	2.2	262.8	0.9	27.3	3.1	263.3	2.6	27.7
E(10)-E(9)	0.3	1.9	3.0	44.3	1.2	2.4	4.7	44.7
E(11)-E(10)	310.3	248.2	419.7	2.3	311.2	248.7	421.4	2.7
E(12)-E(11)	9.8	2.3	1.1	30.8	10.7	2.8	2.8	31.2
E(13)-E(12)	198.7	2679.9	447.8	78.5	199.6	2680.4	449.5	78.9
E(14)-E(13)	0.5	1.6	2.3	1.1	1.4	2.1	4.0	1.5
E(15)-E(14)	211.2	263.2	450.0	142.3	212.1	263.7	451.7	142.7

of the four initial multiexciton states separately. This is shown in Figs. 5–8. Energy separations between the transitions of (3,3) multiexciton as they vary with QD morphology are given in Table II for the emission from α and β states and in Table III for the emission from γ and δ states. It seems that the shape of the QD determines the distances between certain peaks. For example, for lens-shaped and elongated-lens-shaped QDs, distances E(2)-E(1), E(5)-E(4), and E(8)-E(7) are on the order of several meV. However, for truncated cone QD these distances are on the order of several tens of μeV. Interestingly, similar situation occurs for distances between peaks for XX^{+1} transition, where E(2)-E(1) is on the order of several meV for Dot A, Dot C, and Dot D (i.e., lens and elongated lens), but is on the order of several tens μeV for Dot B (truncated cone). This conclusion for XX^{+1} was tested on a library of 240 QDs used in Ref. 20.

2. P_e-P_h recombination channel

In the case of the P recombination channel, P electron recombines with P hole, as shown in Fig. 9. The initial multiplets are four single degenerate levels with dominant configuration $h_0^2h_1^1e_0^2e_0^1$. The final many-particle state is the biexciton ground state, corresponding to a single multiplet due to the h^2e^2 majority character. The $(3,3)\rightarrow(2,2)$ decay in-

TABLE III. Energy separations between the transitions of (3,3) multiexciton as they vary with QD morphology for emission from γ and δ states (see Figs. 7 and 8). Energies are given in μeV.

	Transitions from γ				Transitions from δ			
Trans	Dot A	Dot B	Dot C	Dot D	Dot A	Dot B	Dot C	Dot D
E(2)-E(1)	2880.8	161.1	3207.5	2091.6	2890.7	166.0	3230.8	2095.5
E(3)-E(2)	675.2	169.3	1247.5	2103.5	685.1	174.2	1270.8	2107.4
E(4)-E(3)	162.5	1710.3	225.2	84.4	172.4	1715.2	248.5	88.3
E(5)-E(4)	4276.2	167.4	6546.0	8406.6	4286.1	172.3	6569.3	8410.5
E(6)-E(5)	108.9	3697.4	226.3	91.6	118.8	3702.3	249.6	95.5
E(7)-E(6)	105.6	390.9	219.2	92.1	115.5	395.8	242.5	96.0
E(8)-E(7)	3077.8	169.8	3737.6	7420.6	3087.7	174.7	3760.9	7424.5
E(9)-E(8)	107.5	419.3	217.3	109.8	117.4	424.2	240.6	113.7
E(10)-E(9)	105.6	158.4	219.4	126.8	115.5	163.3	242.7	130.7
E(11)-E(10)	415.6	404.7	636.1	84.8	425.5	409.6	659.4	88.7
E(12)-E(11)	115.1	158.8	217.5	113.3	125.0	163.7	240.8	117.3
E(13)-E(12)	304.0	2836.4	664.2	161.0	313.9	2841.3	687.5	164.9
E(14)-E(13)	105.8	158.1	218.7	83.6	115.7	163.0	242.0	87.5
E(15)-E(14)	316.5	419.7	666.4	224.8	326.4	424.6	689.7	228.7

volves two dark transitions (transitions 1 and 2 in Fig. 9) and two allowed transitions (transitions 3 and 4 in Fig. 9). Interestingly, on the low-resolution emission spectra (see Sec. II B), and according to the perturbation theory (Fig. 2), this transition is considered to be a singlet, but the full calculations show two optically active transitions split by ~ 10 μeV. Energy separations between the transitions in the P recombination channel of (3,3) multiexciton as they vary with QD morphology are shown in the Table within Fig. 9.

D. $XXXX^0_{4,4}$: Neutral four-exciton (Figs. 10 and 11)

As in the case of the spectrum of the (3,3) multiexciton, there are two principal radiative decay channels for $(4,4) \rightarrow (3,3)$, corresponding to the recombination of either an exciton from S shell or an exciton from the P shell. The oscillator strength from the recombination of S (P) electron with P (S) hole is very weak, therefore, not considered here.

1. S_e-S_h recombination channel

The initial single-particle configuration is $h_0^2 h_1^2 e_0^2 e_1^2$, i.e., both electron and hole S and P shells are closed, thus the net spin is zero (Fig. 10).[29] The final single-particle configuration is $h_0^1 h_1^2 e_0^1 e_1^2$, which allows for four different spin configurations. The initial multiparticle state is single multiplet. The total multiplicity of the final multiparticle state is four, with four levels, all dominated by $h_0^1 h_1^1 e_0^1 e_1^1$ configuration. The $(4,4) \rightarrow (3,3)$ decay involves two allowed transitions (denoted as transitions 1 and 2 in Fig. 10) and two dark transitions (denoted as transitions 3 and 4 in Fig. 10). Dependence of the energy differences between the four peaks in the spectrum of (4,4) multiexciton on the QD structural properties is shown in the Table within Fig. 10.

2. P_e-P_h recombination channel

In the case of P recombination channel, a P electron recombines with a P hole, as shown in Fig. 11. The initial multiplet is a singly degenerate level with a dominant configuration $h_0^2 h_1^2 e_0^2 e_0^2$. The final many-particle state is a triexciton ground state corresponding to four multiplets due to $h_0^2 h_1^1 e_0^2 e_1^1$ majority character. The $(4,4) \rightarrow (3,3)$ decay involves two allowed transitions (transitions 1 and 2 in Fig. 11) and two dark transitions (transitions 3 and 4 in Fig. 11). Energy separations between the transitions in the spectrum of (4,4) multiexciton as they vary with QD morphology are given in the Table within Fig. 11.

V. NEGATIVELY CHARGED (MULTI)EXCITONS

When a dot gets charged with N_h holes and N_e electrons, such that $N_e > N_h$, the negatively charged (multi)excitons are formed. Figures 12–15 show schematic plot of the internal structure and FSS of (N_h, N_e) multiexciton for $N_e = N_h + 1$, where $N_h = 1, 2, 3$.

The schematic transitions illustrated in Figs. 12–15 pertain to a generic self-assembled QD and are of general validity according to our calculations. The specific energy separations between transition lines are determined by structural parameters of QDs [shown in the Tables within the figures

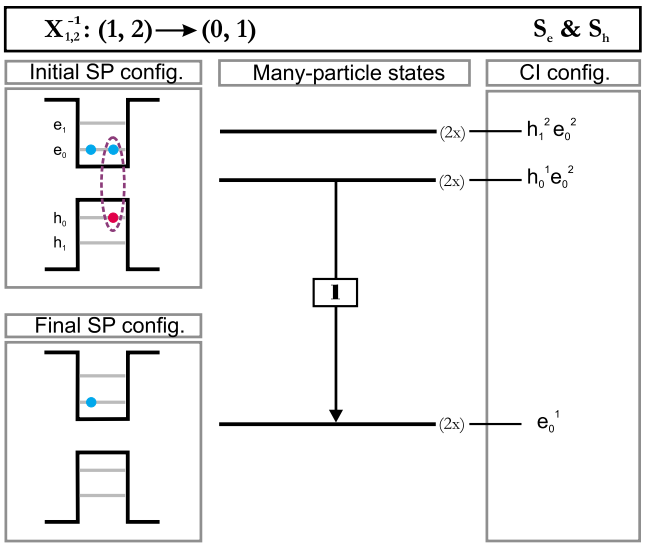

FIG. 12. (Color online) Schematic plot of the internal electronic structure of negatively charged exciton ($N_h = 1$, $N_e = 2$). As in the case of figures for neutral multiexcitons the title indicates the transition [e.g., $(1,2) \rightarrow (0,1)$] and the recombination channel. The left panels give the initial single-particle levels, e.g., $h_0^1 e_0^2$ and the final single-particle level, e.g., e_0^1; the dotted ellipse indicates the e-h pair that recombines. The center panels give the initial many-particle multiplets and final many-particle multiplets and their multiplicities. On the RHS we give the dominant CI configuration denoted as $h_0^{n0} h_1^{n1} \ldots h_j^{nj} e_0^{m0} e_1^{m1} \ldots e_i^{mi}$, where i and j denote electron and hole levels, respectively, and $mj(ni)$ denote the number of electrons (holes) on level $i(j)$ ($0 \leq ni$, $mj \leq 2$). The vertical arrows connecting final and initial multiplets show the multiexcitonic transition.

for each negatively charged (multi)exciton, where the energies are given in μeV] and also by random-alloy fluctuations (see Sec. VII). We provide numerical results for four prototypical structures and note that all other inspected structures follow this range.

A. $X^{-1}_{1,2}$: Negatively charged exciton (Fig. 12)

When a QD gets loaded with two electrons and one hole, a negatively charged exciton or a negative trion is formed. The initial single-particle level is $h_0^1 e_0^2$ and the final level is e_0^1. The initial multiplet state of $X^{-1}_{1,2}$ consists of one doubly degenerate state (because the hole S shell is partially occupied giving 2^1 different spin configurations). The total spin of a trion has a half-integer value. The final multiplet state has one doubly degenerate state dominated by the e_0^1 configuration. The $(1,2) \rightarrow (0,1)$ decay involves one transition, which is optically active and denoted as transition 1 in Fig. 12. This transition does not have a fine structure.

B. $XX^{-1}_{2,3}$: Negatively charged biexciton (Fig. 13)

In the case of negatively charged biexciton XX^{-1}, the single-particle S-electron and S-hole levels are fully occupied, and the P electron level is only partially occupied, as shown in Fig. 13. The final single-particle configuration is $h_0^1 e_0^1 e_1^1$, which allows for 2^3 spin configurations. The initial

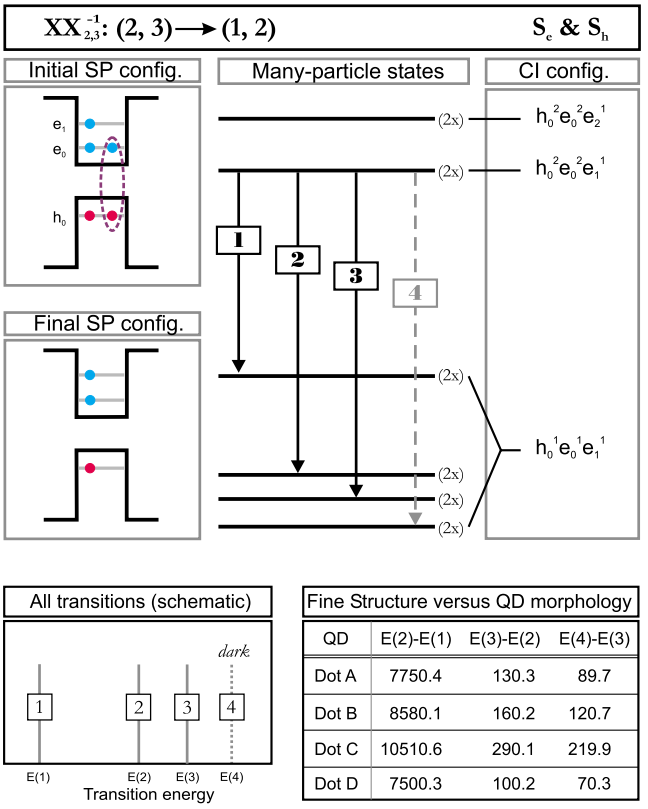

Fine Structure versus QD morphology			
QD	E(2)-E(1)	E(3)-E(2)	E(4)-E(3)
Dot A	7750.4	130.3	89.7
Dot B	8580.1	160.2	120.7
Dot C	10510.6	290.1	219.9
Dot D	7500.3	100.2	70.3

FIG. 13. (Color online) Schematic plot of the internal electronic structure of negatively charged biexciton (N_h=2, N_e=3).

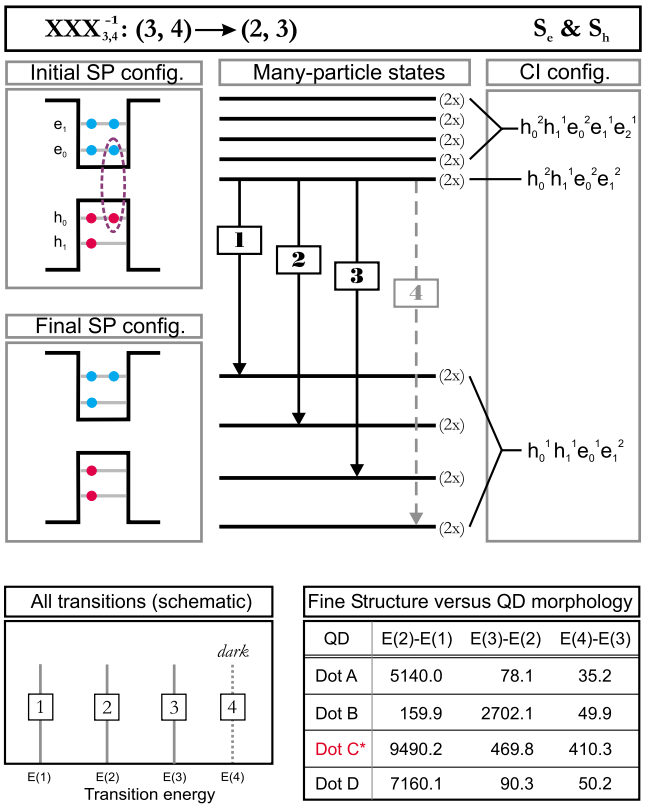

Fine Structure versus QD morphology			
QD	E(2)-E(1)	E(3)-E(2)	E(4)-E(3)
Dot A	5140.0	78.1	35.2
Dot B	159.9	2702.1	49.9
Dot C*	9490.2	469.8	410.3
Dot D	7160.1	90.3	50.2

FIG. 14. (Color online) Schematic plot of the internal electronic structure of negatively charged three-exciton (N_h=3, N_e=4). The S recombination channel of (3,4)→(2,3) transition is shown.

multiplet state of $XX^{-1}_{2,3}$ consists of one doubly degenerate state and the final multiplet state has four doubly degenerate states, all dominated by $h^1_0e^1_0e^1_1$ configuration. The (2,3)→(1,2) decay involves three allowed transitions (denoted as transitions 1, 2, and 3 in Fig. 13), and one dark transition (denoted as transition 4 in Fig. 13). Dependence of the energy difference between the four peaks in the spectrum of the (2,3) multiexciton on the QD structural properties is shown in the Table within Fig. 13. One can see from the Table that transitions 1 and 2 are grouped together, whereas transition 1 is shifted typically by ~10 meV for all four model QDs.

C. $XXX^{-1}_{3,4}$: Negatively charged triexciton (Figs. 14 and 15)

The negatively charged triexciton has both electron and hole P shells occupied, so the P recombination channel (beside the S recombination channel) exists.

1. S_e-S_h recombination channel

The initial single-particle configuration is $h^2_0h^1_1e^2_0e^2_1$, i.e., only the hole P shell is partially occupied. The final single-particle configuration is $h^1_0h^1_1e^1_0e^2_1$, which allows for 2^3=8 different spin configurations. The initial multiparticle state is doubly degenerate multiplet. The total multiplicity of the final multiparticle state is eight, with four doubly degenerate states, all dominated by the $h^1_0h^1_1e^1_0e^2_1$ configuration. The (3,4)→(2,3) decay involves three allowed transitions (denoted as transitions 1, 2, and 3 in Fig. 14) and one dark transition (denoted as transition 4 in Fig. 14). Dependence of the energy difference between the four peaks in the spectrum of the (3,4) multiexciton on the QD structural properties is shown in the Table within Fig. 14.

Interestingly, Dot C (denoted with asterisk in Fig. 14) does not have Aufbau occupation of electron levels in the

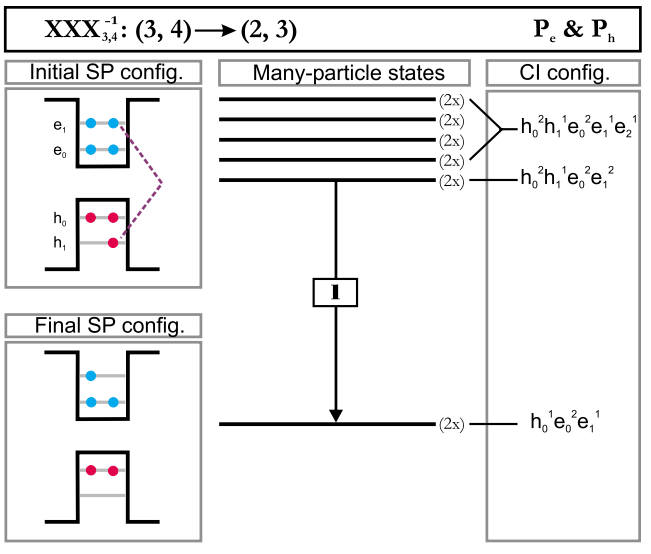

FIG. 15. (Color online) Schematic plot of the internal electronic structure of negatively charged three-exciton (N_h=3, N_e=4). The P recombination channel of (3,4)→(2,3) transition is shown.

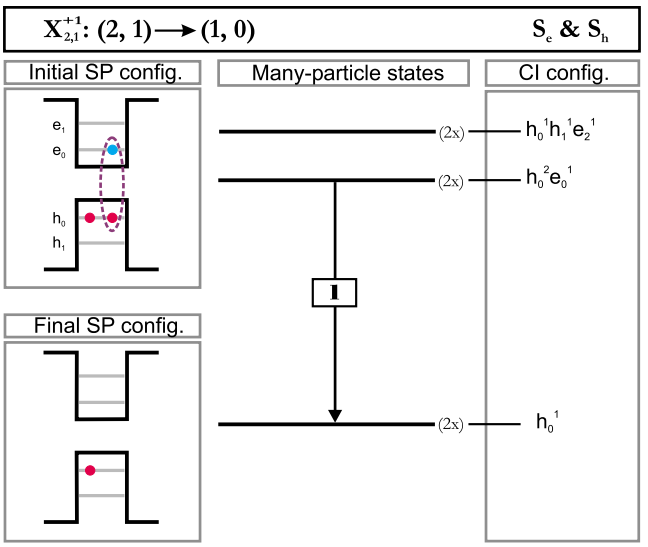

FIG. 16. (Color online) Schematic plot of the internal electronic structure of positively charged exciton (N_h=2, N_e=1). As in the case of figures for neutral multiexcitons the title indicates the transition [e.g., (2,1)→(1,0)] and the recombination channel. The left panels give the initial single-particle levels, e.g., $h_0^2e_0^1$, and the final single-particle level, e.g., h_0^1; the dotted ellipse indicates the e-h pair that recombines. The center panels give the initial many-particle multiplets and final many-particle multiplets and their multiplicities. On the RHS we give the dominant CI configuration denoted as $h_0^{n0}h_1^{n1}\ldots h_j^{nj}e_0^{m0}e_1^{m1}\ldots e_i^{mi}$, where i and j denote electron and hole levels, respectively, and $mj(ni)$ denote the number of electrons (holes) on level $i(j)$ ($0\leq ni$, $mj\leq 2$). The vertical arrows connecting final and initial multiplets show the multiexcitonic transition.

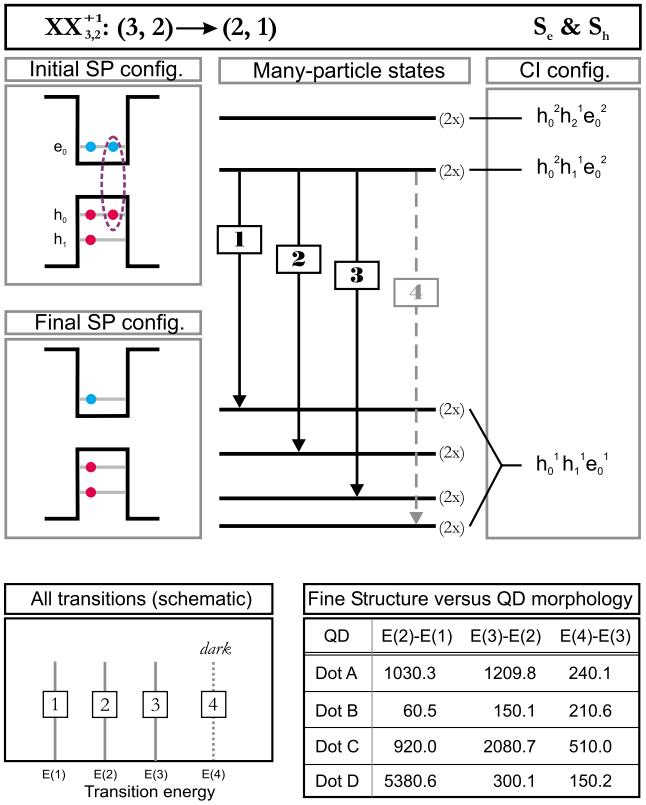

FIG. 17. (Color online) Schematic plot of the internal electronic structure of positively charged biexciton (N_h=3, N_e=2).

initial (3,4) state. Because of the relatively small P-shell electron splitting (see Table I), it is energetically more favorable for the fourth electron to occupy the second P level than the first P shell. In the multiparticle picture, this leads to the initial state with the dominant configuration $h_0^2h_1^1e_0^2e_1^1e_2^1$, with four doubly degenerate levels (the multiplicity of the charged triexciton is 2^3=8). The dominant configuration of the final state is $h_0^1h_1^1e_0^1e_1^1e_2^1$, with a total multiplicity of 2^5=32. Thus, the emission spectrum of the non-Aufbau (3,4) multiexciton has 128 transitions. However, if Dot C gets charged with one more hole [which corresponds to the case of (4,4) multiexciton], then the electron levels restore Aufbau occupation, i.e., the dominant configuration of the initial multiexciton state becomes $h_0^2h_1^2e_0^2e_1^2$ (see Sec. IV D).

2. P_e-P_h recombination channel

In the case of the P recombination channel, P electron recombines with P hole, as shown in Fig. 15. The initial multiplets are four singly degenerate multiplets with dominant configuration $h_0^2h_1^1e_0^2e_1^2$. The final many-particle state is the negatively charged biexciton ground state, corresponding to a doubly degenerate multiplet due to $h_0^2e_0^2e_1^1$ majority character. The (3,4)→(2,3) decay involves one transition that is also optically active (Fig. 15). This transition does not have a fine structure. As in the case of S recombination channel, Dot C does not have Aufbau occupation of the electron levels in the initial (3,4) state, but instead it has a state with dominant configuration $h_0^2h_1^1e_0^2e_1^1e_2^1$. The final multiexciton state has thus the dominant configuration of $h_0^2e_0^2e_2^1$. This gives in total of one doubly degenerate final level. The P channel of the emission from Dot C (3,4) multiexciton has four transitions (one dark and three optically active).

VI. POSITIVELY CHARGED (MULTI)EXCITONS

When a dot gets charged such that $N_e<N_h$, positively charged (multi)excitons are formed. Figures 16–19 show schematic plot of the internal structure and FS of (N_h,N_e) multiexciton for $N_h=N_e+1$, where N_e=1,2,3.

The schematic transitions illustrated in Figs. 16–19 pertain to a generic self-assembled QD and are of general validity according to our calculations. The specific energy separations between transition lines are determined by structural parameters of QDs [shown in Tables within the figures for each positively charged (multi)exciton, where the energies are given in μeV] and also by random-alloy fluctuations (see Sec. VII). We provide numerical results for four prototypical structures and note that all other inspected structures follow this range.

A. $X_{2,1}^{+1}$: Positively charged exciton (Fig. 16)

When a QD gets loaded with one electron and two holes, positively charged exciton (trion), is formed. The initial single-particle level is $h_0^2e_0^1$ and the final single-particle level is h_0^1. The initial multiplet state of $X_{2,1}^{+1}$ consists of one double

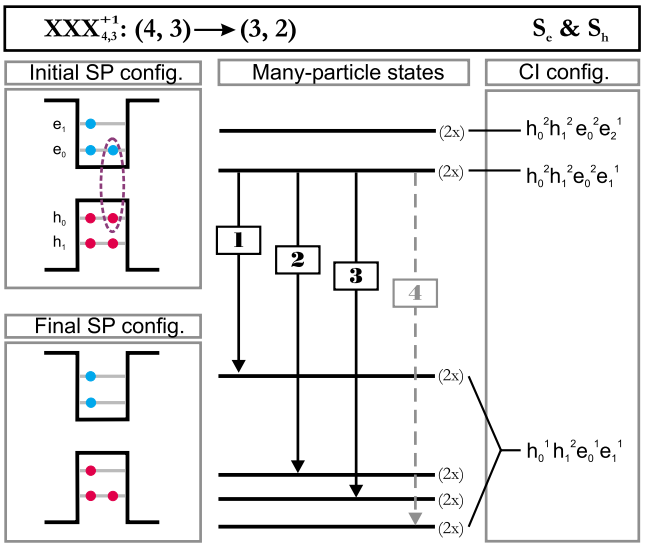

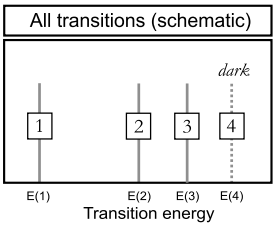

Fine Structure versus QD morphology

QD	E(2)-E(1)	E(3)-E(2)	E(4)-E(3)
Dot A	7349.8	120.3	70.4
Dot B	8309.8	130.1	110.2
Dot C	10750.4	179.9	180.1
Dot D	7160.1	90.3	50.2

FIG. 18. (Color online) Schematic plot of the internal electronic structure of positively charged three-exciton (N_h=4, N_e=3). The S recombination channel of $(4,3)\rightarrow(3,2)$ transition is shown.

degenerate state because the electron S shell is partially occupied giving 2^1 different spin configurations. The total spin of a trion has a half-integer value. The final multiplet state has one doubly degenerate state dominated by the h_0^1 configuration. The $(2,1)\rightarrow(1,0)$ decay involves one transition, which is optically active, and denoted as transition 1 in Fig. 16. This transition does not have a fine structure.

We analyze here a ground-state trion (where electrons and holes occupy the ground state of the QD). However, it is possible that one of two holes occupies the first or higher excited state, leading to the formation of a so-called "hot trion." For example, the dominant configuration of a hot trion can be $h_0^1h_1^1e_0^1$. The fine structure of such a hot trion is much more complex given that there are 2^3 different spin configurations (see, e.g., Ref. 30).

B. $XX^{+1}_{3,2}$: Positively charged biexciton (Fig. 17)

Figure 17 shows the internal electronic structure and FSS of the positively charged biexciton XX^{+1}. The initial single-particle configuration is $h_0^2h_1^1e_0^2$ (with 2^1 different spin configurations), and the final is $h_0^1h_1^1e_0^1$ (with 2^3 spin configurations). The initial multiparticle state is a doubly degenerate multiplet. The total multiplicity of the final state is eight, with four doubly degenerate levels, all dominated by the $h_0^1h_1^1e_0^1$ configuration. The $(3,2)\rightarrow(2,1)$ decay involves three optically active transitions (denoted as transitions 1, 2, and 3 in Fig. 17) and one dark (transition 4 in Fig. 17). Dependence of the energy difference between the four peaks in the spectrum of the (2,3) multiexciton on the QD structural properties is shown in the Table within Fig. 17. Interestingly, whereas transitions 2 and 3 were very close to each other in energy (within 300 μeV) and transition 1 was redshifted by $\sim$10 meV in the spectrum of the negatively charged biexciton, (2,3), such grouping does not exist in the spectrum of positively charged biexciton (3,2), which exhibits a remarkable dependence on QD morphology. For example, whereas in Dot B transitions are separated energetically by a few tens of μeV, for the case of Dot D, transition 1 is redshifted from transitions 2 and 3 by $\sim$5 meV, i.e., three optically active transitions are grouped similar as in the spectrum of (2,3) multiexciton.

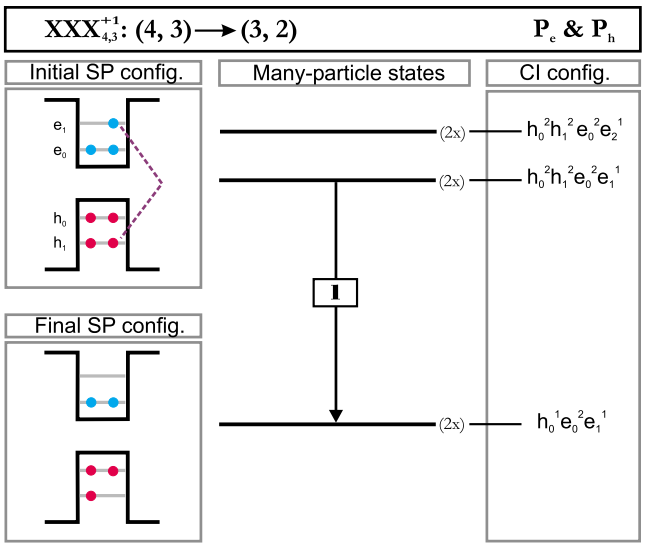

FIG. 19. (Color online) Schematic plot of the internal electronic structure of positively charged three-exciton (N_h=4, N_e=3). The P recombination channel of $(4,3)\rightarrow(3,2)$ transition is shown.

C. $XXX^{+1}_{4,3}$: Positively charged three-exciton (Figs. 18 and 19)

Just as in the case of neutral multiexcitons and negatively charged multiexcitons with $N_h, N_e > 2$, beside S recombina-

TABLE IV. Neutral exciton energy (E_X^0) and energy separations between the transitions in the spectrum of (1,1) exciton, as they vary with three different RRs, σ_1, σ_2, and σ_3. In the Table within Fig. 3, energy separations are shown for RR=σ_1.

$X^0_{1,1}$	σ	Dot A	Dot B	Dot D
E_X^0 (eV)	σ_1	1.255	1.101	1.198
	σ_2	1.250	1.092	1.197
	σ_3	1.252	1.098	1.195
E(2)-E(1) (μeV)	σ_1	142.1	173.5	97.6
	σ_2	141.2	178.3	99.3
	σ_3	144.6	178.9	97.5
E(3)-E(2) (μeV)	σ_1	3.0	1.1	4.1
	σ_2	10.3	4.1	9.2
	σ_3	13.1	2.2	3.9

TABLE V. Energy separations (ΔE) between transitions in the spectra of $XX^{-1}_{2,3}$, $XXX^{0}_{3,3}$, and $XXX^{+1}_{4,3}$ multiexcitons as they vary with three different RRs, σ_1, σ_2, and σ_3. In the Tables within Figs. 4–19, energy differences are shown for RR=σ_1.

Multiexciton	ΔE	σ	Dot A	Dot B	Dot D
$XX^{-1}_{2,3}$ (S_e&S_h)	E(2)-E(1) (μeV)	σ_1	7750.4	8580.1	7500.3
		σ_2	7980.2	9059.6	7619.9
		σ_3	8397.9	8740.3	7580.2
	E(3)-E(2) (μeV)	σ_1	130.3	160.2	100.2
		σ_2	129.9	170.0	100.0
		σ_3	130.4	170.2	99.8
	E(4)-E(3) (μeV)	σ_1	89.7	120.7	70.3
		σ_2	100.3	120.0	80.4
		σ_3	100.4	12.3	71.1
$XXX^{0}_{3,3}$ (P_e&P_h)	E(2)-E(1) (μeV)	σ_1	0.9	0.5	0.4
		σ_2	0.6	0.3	0.2
		σ_3	0.2	0.2	0.3
	E(3)-E(2) (μeV)	σ_1	102.9	149.7	90.2
		σ_2	101.2	174.0	90.5
		σ_3	91.3	169.8	80.2
	E(4)-E(3) (μeV)	σ_1	9.9	10.5	4.0
		σ_2	10.2	0.9	9.8
		σ_3	9.8	2.2	10.4
$XXX^{+1}_{4,3}$ (S_e&S_h)	E(2)-E(1) (μeV)	σ_1	7349.8	8309.8	7160.1
		σ_2	7619.9	8717.6	7290.2
		σ_3	7761.2	8480.2	7259.9
	E(3)-E(2) (μeV)	σ_1	120.3	130.1	90.3
		σ_2	120.2	120.4	90.6
		σ_3	120.0	138.8	89.8
	E(4)-E(3) (μeV)	σ_1	70.4	110.2	50.2
		σ_2	69.9	99.7	62.2
		σ_3	80.2	129.2	48.7

tion channel there is the P radiative decay channel, where P electrons recombine with P hole.

1. S_e-S_h recombination channel

The initial single-particle configuration is $h_0^2h_1^2e_0^2e_1^1$, i.e., only electron P shell is partially occupied. The final single-particle configuration is $h_0^1h_1^2e_0^1e_1^1$, which allows for $2^3=8$ different spin configurations. The initial multiparticle state is doubly degenerate multiplet. The total multiplicity of the final multiparticle state is eight, with four doubly degenerate levels, all dominated by the $h_0^1h_1^2e_0^1e_1^1$ configuration. The $(4,3)\rightarrow(3,2)$ decay involves three allowed transitions (denoted as transitions 1, 2, and 3 in Fig. 18) and one dark (denoted as transition 4 in Fig. 18). Dependence of the energy difference between four peaks in the spectrum of (4,3) multiexciton on QD structural properties is shown in the Table within Fig. 18.

2. P_e-P_h recombination channel

In the case of the P recombination channel, P electron recombines with P hole, as shown in Fig. 19. The initial multiplets are four single degenerate levels with dominant configuration $h_0^2h_1^2e_0^2e_1^1$. The final many-particle state is the negatively charged biexciton ground state, corresponding to a doubly degenerate multiplet due to $h_0^2h_0^1e_0^2$ majority character. The P channel $(4,3)\rightarrow(3,2)$ decay involves one transition that is also optically active (Fig. 19). This transition does not have a fine structure.

VII. ROLE OF ATOMIC-SCALE RANDOMNESS

(In,Ga)As QDs are usually alloyed as revealed by structural characterization techniques.[31,32] This fact implies that there is a set of possible spatial configurations,[33] σ, and each can have a distinct property P(σ).[34] What particular spatial configuration σ each QD from an ensemble will have is unknown, and cannot be controlled. In this section we discuss how such atomic-scale randomness [i.e., different random realizations (RRs) of an alloy] influences the internal electronic structure and FS of multiexcitons analyzed in the previous sections.

We show the effect of atomic-scale randomness on the internal structure and FS of four (multi)excitons ($X^0_{1,1}$, $XX^{-1}_{2,3}$,

$XXX^0_{3,3}$, and $XXX^{+1}_{4,3}$) considering three independent alloy random realizations in Dot A, Dot B, and Dot C model QDs (dot D is not alloyed). Whereas we already discussed how different RRs influence the polarization directions of several multiexcitonic transitions,[26] here we show how RRs influence the internal structure and FSS.

Table IV shows how the exciton energy (E^0_X) and FS vary with different RRs. For example, we see that for Dot A, E(3)-E(2) (Fig. 3) varies more than a factor of four with σ. Table V shows how the internal structure and FS of $XX^{-1}_{2,3}$, $XXX^0_{3,3}$, and $XXX^{+1}_{4,3}$ multiexcitons vary with three different RRs. Interestingly, whereas the sequence of the lines is kept, the distances between peaks are very sensitive to RRs.

The atomic-scale randomness is an uncontrollable effect. However, establishing deterministic link between structure and spectra (in general, structure and physical property) in QDs is crucial as nanotechnology attempts to create QDs with tailored properties. This is a very complex problem because QDs (or nanosystems in general) consist of a large number of atoms (often 10^5 atoms), so the complexity of structure prohibits experimental characterization of the full atomistic structure of the morphology.[31] Given that establishing structure-spectra links should be deterministic and that atomic-scale randomness cannot be controlled, it is very important to identify those features in the spectra that are sensitive to the atomic-scale randomness.

We recently proposed[20,35] a procedure (spectral barcoding) to establish structure-spectra relationship in QDs. The procedure is based on deciphering structural information from a sequence of multiexciton lines in the spectra.[20] However, for the spectral barcoding procedure to work, it is important to identify those features of emission spectra that can be linked deterministically to the structural motifs, and exclude those that are uncontrollable, e.g., influenced by the atomic-scale alloy randomness.[26] Thus, as Tables I and IV show, distances between peaks cannot be used to gauge structural information.

VIII. SUMMARY

We provided a detailed account of the genesis of observable many-electron multiples from (dominant) single-particle levels in the self-assembled QDs by performing a detailed theoretical study. For each of the leading (N_h,N_e) excitonic complexes we showed the single-particle configuration and then the many-particle multiplet levels for the initial state of emission (N_h,N_e) and the final state of emission $(N_h-1,\ N_e-1)$. We denoted which states are dark and which are bright; the order and multiplicity, the leading single-particle character of each multiplet state, and the FSS. The schematic transitions for multiexcitons pertain to a generic self-assembled QD and are of general validity according to our calculations. The specific energy separations between transition lines are determined by structural parameters of QDs (shown in Tables within figures for each multiexciton) and also by random-alloy fluctuations. We provide numerical results for four prototypical structures and note that all other inspected structures follow this range. Here the presented information is important and potentially useful for a few reasons: (i) the information serves as a guide for spectroscopic interpretation; (ii) the information reveals non-Aufbau cases, where the dot does not have Aufbau occupation of carriers' levels; (iii) the information shows which transitions are sensitive to random-alloy fluctuations (if the dot is alloyed) and importance of this effect. We show that because of such alloy information, distances between peaks cannot be used to gauge structural information.

ACKNOWLEDGMENTS

This work was funded by the U. S. Department of Energy, Office of Science, under NREL Contract No. DE-AC36-08GO28308. We thank Patanjali Kambhampati for comments on the paper.

*alex.zunger@nrel.gov

[1] R. J. Warburton, C. Schäflein, D. Haft, F. Bickel, A. Lorke, K. Karrai, J. M. Garcia, W. Schoenfeld, and P. M. Petroff, Nature (London) **405**, 926 (2000).
[2] M. Bayer, O. Stern, P. Hawrylak, S. Fafard, and A. Forchel, Nature (London) **405**, 923 (2000).
[3] J.-Y. Marzin, J.-M. Gérard, A. Izraël, D. Barrier, and G. Bastard, Phys. Rev. Lett. **73**, 716 (1994).
[4] M. Grundmann, J. Christen, N. N. Ledentsov, J. Böhrer, D. Bimberg, S. S. Ruvimov, P. Werner, U. Richter, U. Gösele, J. Heydenreich, V. M. Ustinov, A. Yu. Egorov, A. E. Zhukov, P. S. Kop'ev, and Zh. I. Alferov, Phys. Rev. Lett. **74**, 4043 (1995).
[5] B. Urbaszek, R. J. Warburton, K. Karrai, B. D. Gerardot, P. M. Petroff, and J. M. Garcia, Phys. Rev. Lett. **90**, 247403 (2003).
[6] M. S. Skolnick and D. J. Mowbray, Annu. Rev. Mater. Res. **34**, 181 (2004).
[7] S. Rodt, A. Schliwa, K. Pötschke, F. Guffarth, and D. Bimberg, Phys. Rev. B **71**, 155325 (2005).
[8] M. Ediger, G. Bester, A. Badolato, P. M. Petroff, K. Karrai, A. Zunger, and R. J. Warburton, Nat. Phys. **3**, 774 (2007).
[9] E. Poem, J. Shemesh, I. Marderfeld, D. Galushko, N. Akopian, D. Gershoni, B. D. Gerardot, A. Badolato, and P. M. Petroff, Phys. Rev. B **76**, 235304 (2007).
[10] M. Ediger, G. Bester, B. D. Gerardot, A. Badolato, P. M. Petroff, K. Karrai, A. Zunger, and R. J. Warburton, Phys. Rev. Lett. **98**, 036808 (2007).
[11] P. A. Dalgarno, J. M. Smith, J. McFarlane, B. D. Gerardot, K. Karrai, A. Badolato, P. M. Petroff, and R. J. Warburton, Phys. Rev. B **77**, 245311 (2008).
[12] M. E. Ware, E. A. Stinaff, D. Gammon, M. F. Doty, A. S. Bracker, D. Gershoni, V. L. Korenev, Ş. C. Bădescu, Y. Lyanda-Geller, and T. L. Reinecke, Phys. Rev. Lett. **95**, 177403 (2005).
[13] G. Bester, S. Nair, and A. Zunger, Phys. Rev. B **67**, 161306(R) (2003).
[14] P. Hawrylak, Physica E (Amsterdam) **9**, 94 (2001).
[15] A. Zunger, MRS Bull. **23**, 35 (1998).

[16] A. J. Williamson, A. Franceschetri, and A. Zunger, Europhys. Lett. **53**, 59 (2001).
[17] V. Mlinar, A. Franceschetti, and A. Zunger, Phys. Rev. B **79**, 121307(R) (2009).
[18] L. W. Wang and A. Zunger, Phys. Rev. B **59**, 15806 (1999).
[19] A. Franceschetti, L. W. Wang, H. Fu, and A. Zunger, Phys. Rev. B **58**, R13367 (1998).
[20] V. Mlinar and A. Zunger, Phys. Rev. B **80**, 035328 (2009).
[21] R. D. Schaller, M. Sykora, J. M. Pietryga, and V. I. Klimov, Nano Lett. **6**, 424 (2006).
[22] R. D. Schaller and V. I. Klimov, Phys. Rev. Lett. **96**, 097402 (2006).
[23] S. Seidl, B. D. Gerardot, P. A. Dalgarno, K. Kowalik, A. W. Holleitner, P. M. Petroff, K. Karrai, and R. J. Warburton, Physica E (Amsterdam) **40**, 2153 (2008).
[24] A. Franceschetti, H. Fu, L. W. Wang, and A. Zunger, Phys. Rev. B **60**, 1819 (1999).
[25] P. N. Keating, Phys. Rev. **145**, 637 (1966).
[26] V. Mlinar and A. Zunger, Phys. Rev. B **79**, 115416 (2009).
[27] K. Kim, T. B. Norris, and U. Hohenester, J. Appl. Phys. **103**, 113702 (2008).
[28] V. Troncale, K. F. Karlsson, D. Y. Oberli, M. Byszewski, A. Malko, E. Pelucchi, A. Rudra, and E. Kapon, J. Appl. Phys. **101**, 081703 (2007).
[29] *P* shells are not degenerated in the self-assembled QDs, but split by several meV (see, e.g., Ref. 17). Thus, for both electrons and holes, each of the *P* shells can accommodate up to two carriers.
[30] T. Warming, E. Siebert, A. Schliwa, E. Stock, R. Zimmermann, and D. Bimberg, Phys. Rev. B **79**, 125316 (2009).
[31] J. Stangl, V. Holý, and G. Bauer, Rev. Mod. Phys. **76**, 725 (2004).
[32] V. Shchukin, N. N. Ledentsov, and D. Bimberg, *Epitaxy of Nanostructures, Nanoscience and Technology* (Springer, New York, 2003).
[33] A configuration σ is defined as a particular occupation of each of the N lattice sites by either In or Ga atom.
[34] S.-H. Wei and A. Zunger, Appl. Phys. Lett. **56**, 662 (1990).
[35] V. Mlinar, M. Bozkurt, J. M. Ulloa, M. Ediger, G. Bester, A. Badolato, P. M. Koenraad, R. J. Warburton, and A. Zunger, Phys. Rev. B **80**, 165425 (2009).